Materials Science & Engineering C 122 (2021) 111927

Contents lists available at ScienceDirect

Materials Science & Engineering C

journal homepage: www.elsevier.com/locate/msec

Printable alginate/gelatin hydrogel reinforced with carbon nanofibers as electrically conductive scaffolds for tissue engineering

Aleksandra Serafin [a], Caoimhe Murphy [a], Mario Culebras Rubio [a], Maurice N. Collins [b,c,*]

[a] School of Engineering, Bernal Institute, University of Limerick, Limerick, Ireland
[b] Advanced Material and BioEngineering Research Centre (AMBER) and School of Engineering, Bernal Institute, University of Limerick, Limerick, Ireland
[c] Helath Research Institute, University of Limerick, Ireland

ARTICLE INFO

Keywords:
Electroactive
Hydrogels
Tissue engineering

ABSTRACT

Shortages of organs and damaged tissues for transplantation have prompted improvements in biomaterials within the field of tissue engineering (TE). The rise of hybrid hydrogels as electro-conductive biomaterials offers promise in numerous challenging biomedical applications. In this work, hybrid printable biomaterials comprised of alginate and gelatin hydrogel systems filled with carbon nanofibers (CNFs) were developed to create electroconductive and printable 3-D scaffolds. Importantly, the preparation method allows the formation of hydrogels with homogenously dispersed CNFs. These hybrid composite hydrogels were evaluated in terms of mechanical, chemical and cellular response. They display excellent mechanical performance, which is augmented by the CNFs, with Young's moduli and conductivity reaching 534.7 ± 2.7 kPa and $4.1 \times 10^{-4} \pm 2 \times 10^{-5}$ S/cm respectively. CNF incorporation enhances shear-thinning behaviour, allowing ease of 3-D printing. In-vitro studies indicate improved cellular proliferation compared to controls. These conductive hydrogels have the potential to be used in a myriad of TE strategies, particularly for those focused on the incorporation of electroconductive components for applications such as cardiac or neuronal TE strategies.

1. Introduction

Tissue engineering (TE) has been proposed as a possible solution to one of world's greatest challenges; organ donor shortages. In 2010 it was reported that only 10% of the required worldwide organ transplant needs were met, highlighting the necessity for the rapid expansion of TE [1]. This is attributed to the growing numbers in global population, longer life spans and increased incidence of patients with diseased/injured tissue or organ failure [2]. TE ex-vivo scaffolds are constructed and implanted in-vivo to aid the regenerative process. Ideally, the implanted scaffold should aim to match the mechanical stiffness of the surrounding extracellular matrix (ECM), possess the intended cellular ques. and degrade at a similar rate to the rate of regeneration of the targeted tissue.

To achieve this, scaffolds can be developed from a variety of materials, though interest in hydrogels has risen significantly over the years due to their high water content, and their ease of synthesis to produce structures of similar consistency to natural tissue [3]. These hydrogels are often produced from natural polymers such as hyaluronic acid [4] chitosan [5] gelatin or alginate [6], or from synthetic polymers such as poly (acrylic acid) or poly(lactide-co-glycolide) [7].

Often, key drawbacks are associated with low mechanical strengths and fast degradation times, which are some of the important criteria for optimal scaffold performance. Careful selection of crosslinking strategies can largely overcome these drawbacks through tailoring properties such as; stiffness, porosity, degradability and biocompatibility for targeted performance.

Alginate has recently become a favourable material for TE strategies, as well as drug delivery systems, particularly due to its ease of physical crosslinking via ionic interactions. Alginate is composed of 1,4-linked β-D-mannuronic acid (M) and α-L-guluronic acid (G) monomers. Alginate readily crosslinks in the presence of Ca^{2+} ions due to the creation of ionic interchain binding sites between the G blocks of adjacent alginate chains, resulting in a gelled structure. A key downside of using physical crosslinking methods for these materials is poor performance in-vitro and in-vivo, due to the loss of Ca^{2+} ions from the system [8].

Further issues such as poor mechanical properties and inferior cell attachment have directed researchers towards the combination of alginate with other materials [8,9]. Gelatin is often the material of choice for this combination, due to its bioresorbable and biocompatible

* Corresponding author.
E-mail address: Maurice.Collins@ul.ie (M.N. Collins).

https://doi.org/10.1016/j.msec.2021.111927
Received 30 December 2020; Received in revised form 26 January 2021; Accepted 28 January 2021
Available online 3 February 2021

properties, which enable cell adhesion [9–11].

Electrical stimulation, and its importance in cell motility and differentiation, has been known for decades [12–14]. Thus, incorporation of electroconductive elements in scaffolds proves favourable for growth and signalling of surrounding cells [15].

Carbon nanotubes (CNTs) and nanofibers (CNFs) are gaining interest in TE [16–18]. The presence of carbon structures within gels provides a large surface area for electron transfer [17]. CNTs have been investigated and applied to several biomedical technologies including; biosensors [19], drug delivery [20], and in TE scaffolds-particularly for cardiac [21], muscle myofiber [22], neural [23] and bone TE strategies [24]. However, CNTs have shown several cytotoxic problems associated with the presence of metal catalyst impurities used in their synthesis. Their accumulation in organs, cells and tissues is caused by their small size and highly hydrophobic character owing to π-π interactions [25]. In addition, they are usually expensive compared to other carbon nanostructures, limiting their use at a commercial scale. A similarly thorough investigation into the incorporation of CNFs into hydrogels has only recently emerged, in part due to the removal of the necessity to use metal catalysts for their preparation and the possibility of their production from renewable sources, which improves biocompatibility and cell viability [26,27].

The processing of hydrogels for TE application has shifted its attention towards 3D printing mainly because 3D printing offers the possibility of patient specific implants [28]. Its ability to create intricate and complex scaffold geometries gives 3D printing an advantage when compared to standard techniques which require the use of pre-made moulds, dies or other shaping techniques to achieve the desired scaffolds shape. Though highly successful, one of the major challenges facing 3D printing hydrogel scaffolds is the lack of hydrogel systems that can satisfy the viscoelastic properties and crosslinking mechanism required to print scaffolds to a high resolution and with complete shape retention.

Here, we report the preparation of a novel electroconductive hydrogel based on alginate/gelatin with different concentrations of CNFs showing for the first a time a complete study in terms of mechanical, structural, electrical, viscoelastic and cell biocompatibility characterisation. These new CNF hydrogels open future possibilities in terms of improved mechanical and electroconductive properties while allowing the formation of reinforced composite structures post-print. This work represents a breakthrough in the development of multiphase hydrogels for TE applications due to the homogeneous dispersion of CNFs into viscous hydrogel solutions, which allow for a uniform fiber distribution in the hydrogel, a key factor for improved printability, electroactivity and biocompatibility.

2. Experimental

2.1. Materials

Alginic acid sodium salt (M_w = 10,000–600,000 g/mol), gelatin (128-192 Bloom) and calcium chloride were purchased from AppliChem PanReac (Lennox Ireland). CNFs and phosphate buffered saline (PBS) were purchased from Sigma-Aldrich (Ireland). For cell culture experiments, Dulbecco's Modified Minimal Essential Medium (DMEM), L-Glutamine, Penicillin-Streptomycin, Calcein AM and propidium iodine was purchased from Sigma Aldrich (Ireland). Alamar Blue was purchased from Invitrogen (Thermofisher Ireland).

2.2. Preparation of alginate/gelatin/CNFs hydrogels

To prepare the CNF hydrogel, 5% w/v of gelatin was added to deionised water at 50 °C and stirred until fully dissolved. CNFs were then added at varying concentrations; 0.5, 1, 2, 5% w/v, nominated as *Alg-Gel-CNFs-x*, see Table 1, to the dissolved gelatin solution and dispersed by bath sonication for 20 min, tip sonication over an ice bath for 10 min and finally with bath sonication for 20 min. 5% w/v of alginate was subsequently added to the gelatin/CNF hydrogel solution and stirred overnight. Control samples with 0% CNF w/v were synthetised in the same manner, only without the addition of CNF. Hydrogel solutions were poured into circular moulds, 13.5 mm in diameter and 4 mm high and crosslinked in 200 mM $CaCl_2$ solution for 24 h.

Table 1
Composition of the prepared samples.

Sample name	CNF concentration (% w/v)	Alginate (% w/v)	Gelatin (% w/v)
Alg-Gel-CNFs-0	0%	5	5
Alg-Gel-CNFs-0.5	0.5%	5	5
Alg-Gel-CNFs-1	1%	5	5
Alg-Gel-CNFs-2	2%	5	5
Alg-Gel-CNFs-5	5%	5	5

2.3. CNF hydrogel characterisation

Visual analysis of the CNF dispersion within the CNF hydrogel was conducted via SEM analysis with Hitachi SU70 SEM at an imaging voltage of 10 kV. Before the observation, the hydrogels were fabricated as described above, lyophilised with Eurotherm LS40/60, (Severn Science Ltd., Bristol, England) with cooling for 8 h at −30 °C at 100 mbar, first drying for 16 h at −10 °C under 0.1 mbar and secondary drying for 2 h at 20 °C (under vacuum), and subsequently coated with gold sputtering before the SEM analysis.

Compression tests were conducted on CNF hydrogels using an in-house compression test facility equipped with a 1 kN load cell and compressed at a rate of 1 mm/s between parallel plates. The Young's Modulus of the samples was calculated as the slope in the linear region of a normalised stress vs. strain graph.

Resistivity was measured using an Ohm meter. The conductivity of the CNF hydrogel samples was then calculated as follows:

$$\sigma = \frac{l}{RA} \tag{1}$$

where σ is the conductivity, l is the sample length, A is the cross-sectional area and R is the resistance.

Spectra of lyophilised CNF hydrogels were obtained utilising a Spectrum 100 FTIR (PerkinElmer, USA) in the range 650–4000 cm^{-1} for 10 scans.

Prior to swelling tests, CNF hydrogels were dried in a vacuum oven overnight, weighed and then placed in PBS at 37 °C for a period of up to 48 h. Subsequently, the wet weight of the samples was measured, and the swelling degree calculated as follows:

$$\left(\frac{Ws - Wd}{Wd}\right) * 100\% \tag{2}$$

where *Ws* is the hydrogel swollen mass and *Wd* is the dried mass.

Rheological properties were analysed with a hybrid rheometer (TA Instruments, USA), using techniques described in [29]. Briefly, disposable 25 mm aluminium rheological plates were used for the analysis with a measurement gap of 550 μm. The CNF laden samples were tested using the following regimes; 1) strain sweeps ranging from 0.1 to 100% at 1.59 Hz in order to determine the viscoelastic range of the samples, 2) frequency sweeps of 0.1–100 rad/s at the determined constant strain of 2%, 3) steady state flow tests with shear rates ranging from 0.5 to 500 s^{-1} and 4) recovery test under shear rates of 0.1 s^{-1} and 100 s^{-1}. All the experiments were conducted at room temperature.

2.4. 3D printing of CNF hydrogel

Prior to printing scaffolds, 3D models were created using CAD

software (SolidWorks 2016), processed into a printable design by a splicing software (Repetier-Host) and printed with an Allevi 2 Printer (Allevi, USA). Test lattices of the different CNF hydrogels were printed using a printing speed of 4 mm/s. The pressure and temperature parameters inside the printing cylinder were modified for each hydrogel to provide the optimal printing quality. Printed designs were constructed as two layers (2 mm per layer), resulting in structures 4 mm in height and 9 mm in width and subsequently crosslinked for 24 h (Fig. 1).

2.5. Biocompatibility of CNF hydrogel

For cell culture, CNF hydrogels were sterilised by autoclave, followed by UV sterilisation and immersed in DMEM cell culture media in order to reach equilibrium for 72 h at 37 °C.

NIH/3T3 fibroblasts were grown in DMEM supplemented with 10% foetal bovine serum, 1% L-Glutamine and 1% Penicillin-Streptomycin in a 5% CO_2 environment. Cells were seeded onto the pre-conditioned CNF hydrogels at a density of 0.04×10^6 cells/construct in a 24-well plate, supplemented with 1 mL of cell culture media and incubated overnight. For cell cytotoxicity evaluation, Alamar Blue was added at 10% of the volume of the well and incubated for 5 h. Measurement of the cell fluorescent emission was carried out with SynergyMx (BioTek, UK) at wavelength 540/590 nm in 384-well plates. Cells incubated without the presence of hydrogels acted as controls. All experiments were repeated four times over a period of 96 h, and the data is presented as means ± standard deviation. To determine the statistical significance, one-way ANOVA was employed, with the p-value of <0.05 considered as statistically significant. Following the cell culture method described above, fibroblasts were stained with Calcein AM and propidium iodine for fluorescence imaging by means of ImageXpress Micro Spinning Disc Confocal High-Content Imaging System (Molecular Devices) to visualise cell viability and attachment on the CNF hydrogels. Quantitative analysis of the cell viability was completed using the Fuji software.

3. Results and discussion

3.1. Morphological and mechanical characterisation of CNF hydrogels

Upon CNF incorporation, heated gelatin solutions exhibited a colour change from opaque to black and CNFs were well distributed. The viscosity of the hydrogel increased with alginate addition. The CNFs remained stable in suspension with no flocculation observed. When cooled to room temperature, the CNF hydrogels retained their shape.

Fig. 2 shows the cross-section of lyophilised CNF hydrogels. Dispersion of CNF is uniform for all CNF concentrations and aggregates of CNF were not observed in the lyophilised structures. This visual confirmation of CNF dispersibility can be attributed to the production method of the CNF hydrogel, whereby multiple ultrasonication steps, including bath and tip sonication, were used to achieve this result. Dispersibility of CNF is usually achieved with the melt mixing process or sonication, though the latter is mostly effective in low viscosity polymer systems [30]. Therefore, the high degree of dispersibility of the CNF in viscous hydrogel solutions such as the CNF alginate/gelatin hydrogel is of importance to subsequent performance of these hydrogel systems. In addition, the high stability of the CNF hydrogel is attributed to the molecular interactions between CNFs, alginate and gelatin , which inhibits the agglomeration and sedimentation of CNFs.

To determine the mechanical properties of the CNF hydrogel, unconfined compression tests were conducted. The addition of CNF filler material into the hydrogel system correlated with an increase in the Young's Modulus of the hydrogels, with an increase from 395.38 ± 0.68 kPa for the Alg-Gel-CNFs-0 to 534.75 ± 2.7 kPa for the Alg-Gel-CNFs-5 as shown in Fig. 3(a).

The compressibility of the CNF hydrogels increases with the addition of the CNF filler material, as higher concentrations of the CNFs allows for the formation of crosslinked CNF networks inside the hydrogel structure. This occurs by means of coordination chemistry with the $CaCl_2$ crosslinker supplying divalent cations of Ca^{2+} [18].

Similar observations were obtained by Llorens-Gámez and Serrano-Aroca when studying the compressibility of alginate/CNF hydrogel

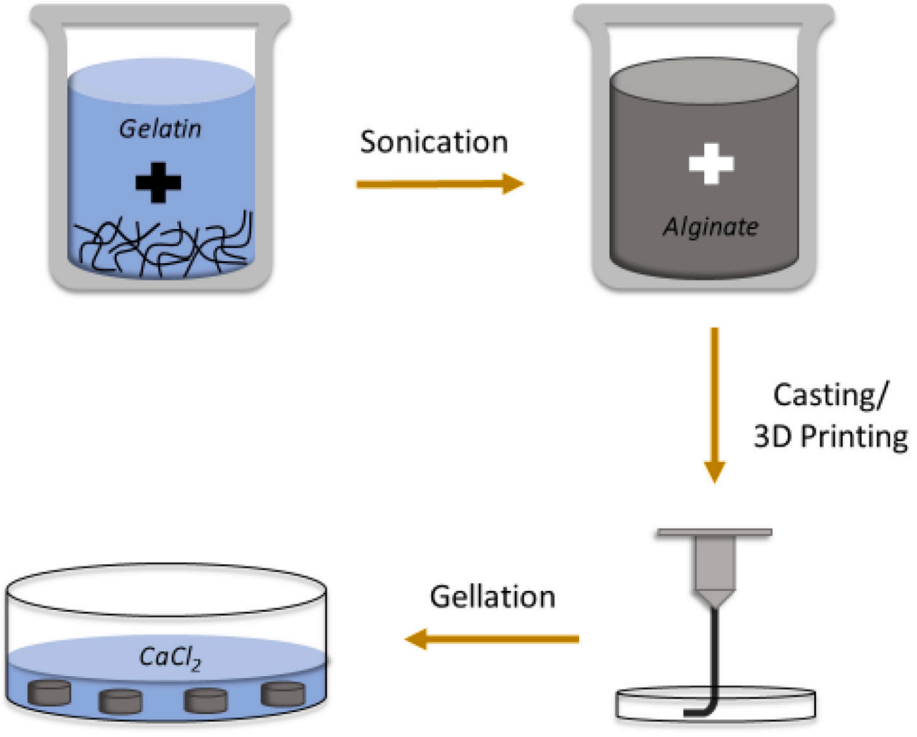

Fig. 1. Schematic of the sample preparation process.

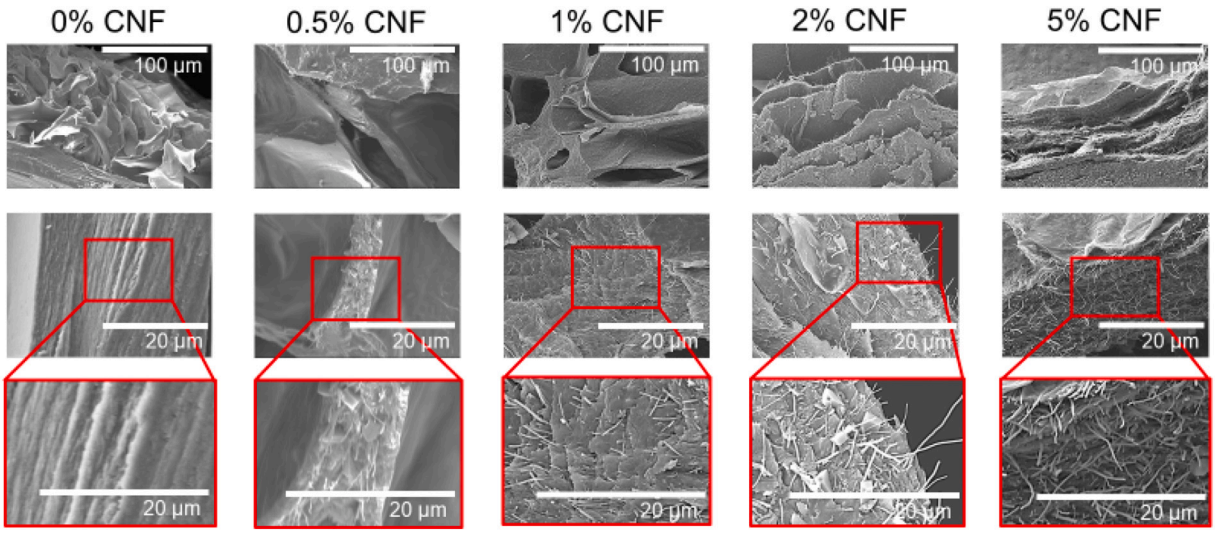

Fig. 2. SEM images of lyophilised hydrogels with different CNFs content. (Top row scale bar 100 µm, middle and bottom row 20 µm.)

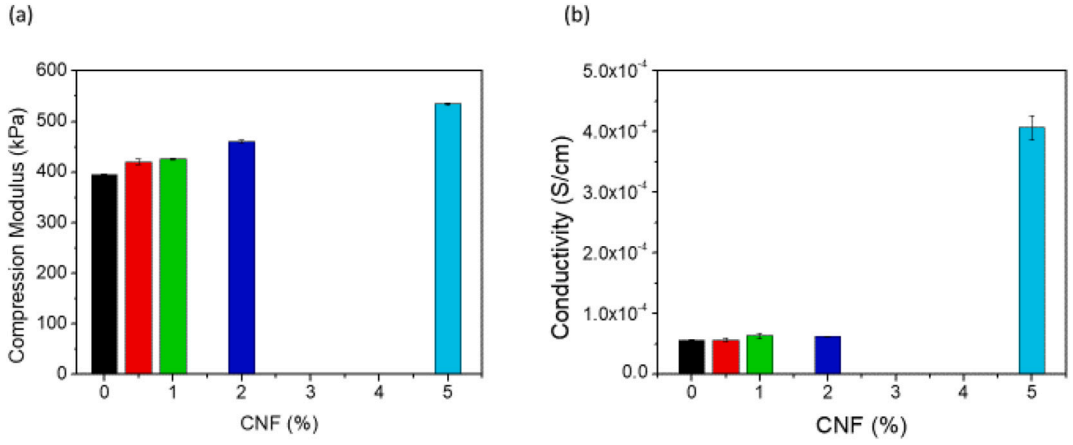

Fig. 3. a) Young's Modulus of the samples of alginate/gelatin/CNFs hydrogels as a function of the CNFs content. b) Electrical conductivity of alginate/gelatin/CNFs hydrogels as a function of the CNFs content.

films with low CNF concentrations crosslinked by metal ion coordination chemistry in the presence of abundant Ca^{2+} ions [18]. This heavily suggests that even a small volume addition of CNFs has the potential to increase the mechanical properties of hydrogel systems to a high degree.

The addition of the CNFs into the hydrogel system is aimed primarily on the improvement of the electroconductive properties, Fig. 3(b) shows the electrical conductivity of the hydrogels as a function of CNFs content. The hydrogels without CNFs (Alg-Gel-CNFs-0) exhibited an

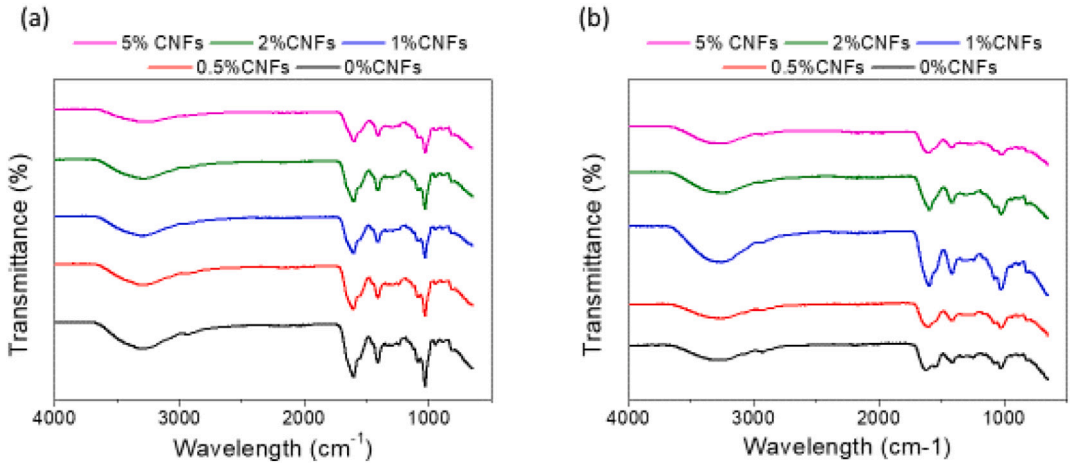

Fig. 4. FTIR of alginate/gelatin/CNFs hydrogels (a) before and (b) after crosslinking.

electrical conductivity of $5.6 \times 10^{-5} \pm 3 \times 10^{-6}$ S/cm. The baseline conductivity of the Alg-Gel-CNFs-0 control arises from the electro-conductive properties of alginate, which has an intrinsic capability to conduct electricity due to the presence of ionic groups. Values for the Alg-Gel-CNFs-0.5, Alg-Gel-CNFs-1 and Alg-Gel-CNFs-2 CNF concentration did not differ significantly from the Alg-Gel-CNFs-0 control (as shown in Fig. 3(b)). However, the conductivity increased to $4.1 \times 10^{-4} \pm 2 \times 10^{-5}$ S/cm for the Alg-Gel-CNFs-5 hydrogel and this is attributed to an increase of the electron conduction transport contribution. However, the results suggest that much higher concentrations of CNFs are required to reach the percolation threshold. Similar values for conductivity were found by [31,32], showcasing that the use of CNFs has as much of an advantageous effect on conductivity as CNTs.

Chemical analysis of the CNF hydrogels with varying CNF concentrations was performed and is shown in Fig. 4, both for crosslinked and non-crosslinked samples. Due to the presence of overlapping bands created by this hydrogel blend, it is difficult to distinguish specific peaks corresponding to individual material components. However, important characteristic absorption band occurs at 1030 cm^{-1} with a shoulder at 1085 cm^{-1}, which relates to C—C and C—O stretching in the alginate. This peak becomes stronger in intensity when the samples are crosslinked, suggesting that Ca^{2+} binds to the guluronic acids in the alginate [6,33,34]. Broadening of the two peaks occurs at 1601 and 1412 cm^{-1} and this is attributed to asymmetric and symmetric stretch vibrations of the ionic binding of the -COO- carboxylic groups in the alginate, indicating that crosslinking occurs successfully.

The peak at 1601 cm^{-1} suggests the presence of an amide I band corresponding to the C—O and C—N stretching of the gelatin, as well as C═C vibration of graphene rings attributed to the presence of CNFs, with these peaks broadening with an increase in the CNF concentration. The peak occurring at 1085 cm^{-1} is also associated with CNFs [6,35,36]. The small peak at 1550 cm^{-1} represents the amide II band while the amide III is visible at 1238 cm^{-1}, representing the C—N stretching and N—H bending corresponding to the presence of gelatin. O—H stretching occurs at the broad absorption band of 3300–3700 cm^{-1} and the C—H band 2850–3000 cm^{-1}, associated with the alginate structure [6,33].

Swelling tests of the CNF laden hydrogels were conducted to determine the crosslinking efficiency. Time dependence of the swelling degree of each CNF hydrogel is shown in Fig. 5(a). Moisture uptake by the CNF hydrogel is most prominent within the first 24 h, after which the swelling began to plateau. Over a period of 48 h, the swelling degree of the Alg-Gel-CNFs-0.5 hydrogel increased to 1610.6 ± 218.9%, while that of the Alg-Gel-CNFs-5 to 807.3 ± 80.3%, as shown in Fig. 5(b), indicating that an increase in the CNF filler concentration diminished the degree of swelling of the hydrogel due to increased crosslinking density.

In alginate based hydrogels crosslinked with Ca^{2+} ions, reversible physical crosslinking is possible due to the diffusion of Ca^{2+} ions from the hydrogel matrix over time, thus allowing the hydrogel to dissolve into the surrounding medium [37,38]. As discussed before, increasing the concentration of the CNF filler allows for the formation of more CNF networks within the hydrogel solution, creating stronger connections between the CNFs and alginate chains [18]. This prevents the physical crosslinking of the hydrogel to be reversed at the higher CNF concentrations, hence retarding the swelling and degradation kinematics.

The rheological properties of CNF laden hydrogels were investigated to analyse their suitability for 3D printing. Storage and loss moduli were analysed over frequencies from 0.1 to 100 rad/s (Fig. 6(a) and (b)). With an increase in the frequency both the storage and the loss moduli increased. The storage modulus remained at a higher value than the loss modulus, indicating that the hydrogels exhibits an elastic (solid like) response.

When applying shear stress, the CNF hydrogel exhibits shear thinning behaviour (Fig. 6(c)). At lower shear rates of 1.25 s^{-1} the Alg-Gel-CNFs-5 exhibits a viscosity of 810.4 Pa·s which is reduced by two orders of magnitude at the higher shear rates of 125 s^{-1}. The same trend can be observed for the other hydrogel samples. Overall, increasing the concentration of the CNFs increased the viscosity of the samples, in line with the other mechanical characterisation tests.

When 3D printing structures which require post printing crosslinking regimes, it is important for the material to maintain the desired shape throughout the printing process, i.e. the material should exhibit shear-thinning behaviour while printing and shape fidelity post-printing. These desired features allow for a rapid decrease in the viscosity with applied shear for printing to occur. Removal of the force rapidly recovers the material, maintaining the printed shape before a crosslinking regime is introduced. Recovery tests of the hydrogels were conducted by applying a low shear rate of 0.1 s^{-1} to the samples for 60 s, mimicking the conditions of the sample inside the printing nozzle. The shear rate was then increased to 100 s^{-1} for 10 s to simulate the shear forces acting on the material as it is printed through the nozzle and decreased again to low shear rate of 0.1 s^{-1} for 60 s to allow the sample to recover after the printing simulation. All hydrogel samples exhibited the desired behaviour, with the viscosity dropping drastically with a sharp increase in the shear rate from 100 s^{-1} to 0.1 s^{-1}. For the case of the Alg-Gel-CNFs-5 hydrogel, the initial viscosity of 15,545.7 Pa·s decreased to 25.8 Pa·s with the instantaneous higher shear value. After 10 s at the lower shear rate, the viscosity recovered to 4694.7 Pa·s, representing a recovery of 30.2% of the initial value. For longer recovery times of 30 and 60 s the recovery was at 31.4% and 32.3% respectively, suggesting that most of the material recovery occurs within the first 10 s after removal of the higher shear rates. This trend was seen for all hydrogel concentrations. A

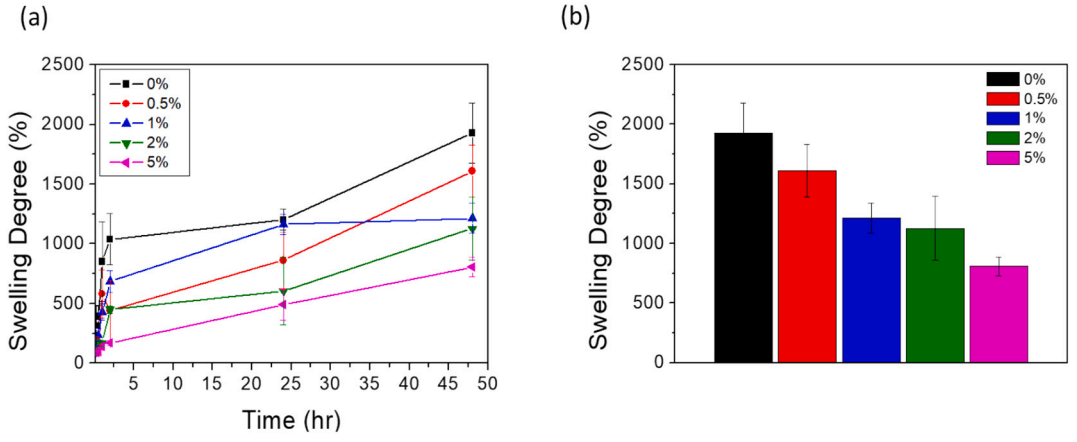

Fig. 5. Swelling properties of the CNFs hydrogels. a) Trend of the swelling degree of the CNFs hydrogels time dependence over a period of 48 h. b) Swelling degree at the 48 h time point.

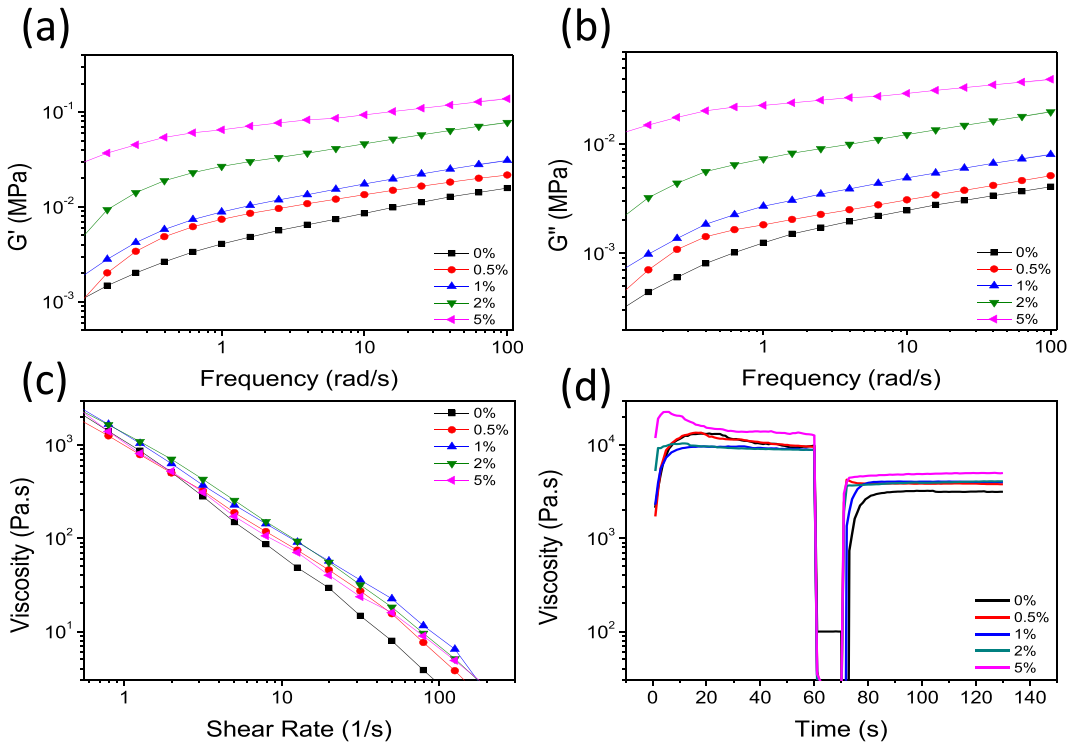

Fig. 6. (a) Storage and (b) loss modules of the hydrogels prepared as a function of frequency. (c) Viscosity dependency of the shear rate and (d) recovery test of the of alginate/gelatin/CNFs hydrogels at different CNFs content.

period of time is required for the hydrogel to recover following the removal of a high shear stress to allow the restoration of the polymer chain alignment within the hydrogel network [29,39].

3.2. 3D printing of CNF hydrogel

Difficulty in printing hydrogels is mainly attributed to their low viscosity behaviour. By introducing the presence of CNFs into an alginate/gelatin system the viscosity of the material increases, allowing for better printing capability. Printed samples of the different CNF laden hydrogels are shown in Fig. 7. All the samples, bar the Alg-Gel-CNFs-5 concentration, could be printed successfully. The Alg-Gel-CNFs-5 was unable to be printed, with multiple breakages in the printed lines, no matter the shape printed.

The pressure and temperature parameters inside the printing cylinder were adjusted for each CNF hydrogel to provide the optimal printing quality. Pressures ranged from 10.6 to 28.6 PSI while temperatures ranged from 22 to 38 °C. It should be noted that cooler temperatures allowed for easier printing with distinctive lines to be achieved. Allowing the material to remain in the printing cylinder over longer periods of time diminished the optimum printing quality, due to the continuous heating of the material. This reduced the viscosity of the material and forced the extruder pressure to be lowered in order to achieve the distinct material lines when printing. This occurrence prevented the establishment of precise printing parameters, though when printing within the established printing window parameters outlined in Table 2, generally 3D printing of CNF hydrogels into the desired geometries was successful.

Table 2
Optimal 3D printing parameter window of CNF hydrogel.

CNF (w/v)	Temperature (°C)	Pressure (PSI)	Printing time (min)
0%	20–25	9.8–14	1–5
0.5%	22–28	10.6–27.6	1–5
1%	25–30	12.6–18.6	1–5
2%	28–30	12.4–28.6	1–5
5%	35–38	13–23	1–5

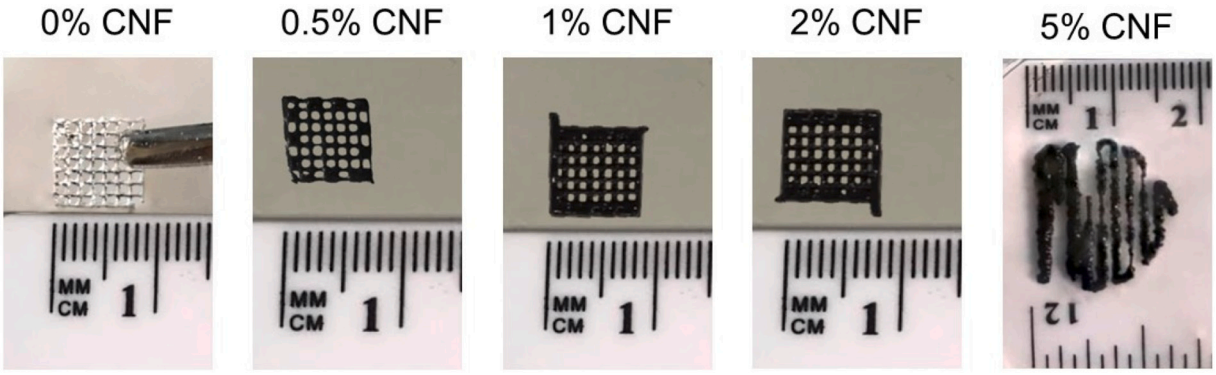

Fig. 7. Images of 3D printed lattices using alginate/gelatin/CNF hydrogels.

3.3. Biocompatibility of CNF hydrogel

The potential cytotoxicity effects of the CNF hydrogels were tested using NIH/3T3 fibroblasts cells by means of Alamar Blue Assay. Cells seeded on top of the hydrogels were tested for their potential to proliferate over a period of 96 h, with the cellular response measured by fluorescence at 24 h time intervals, as presented in Fig. 8(a). After an initial 24 h in culture, the proliferation of cells seeded in the control group without the presence of hydrogels had the most prominent spike in proliferation (75.96 ± 36.03%), while all the CNF hydrogel groups had moderate proliferation ranging from 30.49 ± 5.3% to 47.12 ± 15.86%. Over the following 48 h the proliferation of cells in all groups decreased, though at the 96 h time interval it increased again, suggesting that the cells were adjusting to the presence of the hydrogel material. The proliferation of cells was highest for the Alg-Gel-CNFs-0 group (110.43 ± 56.5%), followed by the Alg-Gel-CNFs-0.5 and Alg-Gel-CNFs-5 groups with similar results (82.83 ± 23.9% and 75.6 ± 25.1%, respectively), with the control exhibiting the smallest numbers of cell proliferation at this time point. One-way ANOVA showed a statistical difference in the proliferation rates of cells between the hydrogel groups and the cell control, though no statistical difference was found between the hydrogel groups themselves.

Cells cultured in the same manner on the CNF hydrogels were also evaluated using a live-dead assay after 96 h in culture. Fluorescent images of the cell were captured with a confocal microscope and presented in Fig. 8(c), where live cells are stained green and dead cells are stained red. High numbers of live cells were observed in all hydrogel groups, with very few dead cells present. The cell percentage viability was quantified by means of Fiji software and presented in Fig. 8(b). Cell viability for all groups ranged above 88%, indicating the biocompatible property of the CNF hydrogels. The cells in all hydrogel groups were similar in their morphology to the cells in the control group, with cell extensions visible on the outskirts of the cell clusters, indicating their proliferating behaviour.

This data suggests that the presence of the CNF hydrogels does not elicit a cytotoxic effect on cultured cells, and in turn suggests that the CNF hydrogels are biocompatible. This can in part be attributed to the presence of cell-adhesive ligands in the gelatin structure which aids in the attachment of the cells to their substrates when compared to the control group cultured on tissue culture plates [10], as well as the increased conductivity of the CNF hydrogels. Various studies have shown that scaffolds which exhibit electro-conductive properties aid in cellular interactions and can be considered as beneficial to the survival, growth and even differentiation of cells, seen particularly in the case of stem cell differentiation into neuronal cells [40–42]. The amount of CNFs in the hydrogel system does not appear to influence the proliferation rates of NIH/3T3 cells to a great extent, though further studies utilising cells of a conductive nature such as neural cells seeded on the CNF hydrogels should be conducted to examine this potential response more thoroughly.

4. Conclusions

This hydrogel preparation method allows for the subsequent

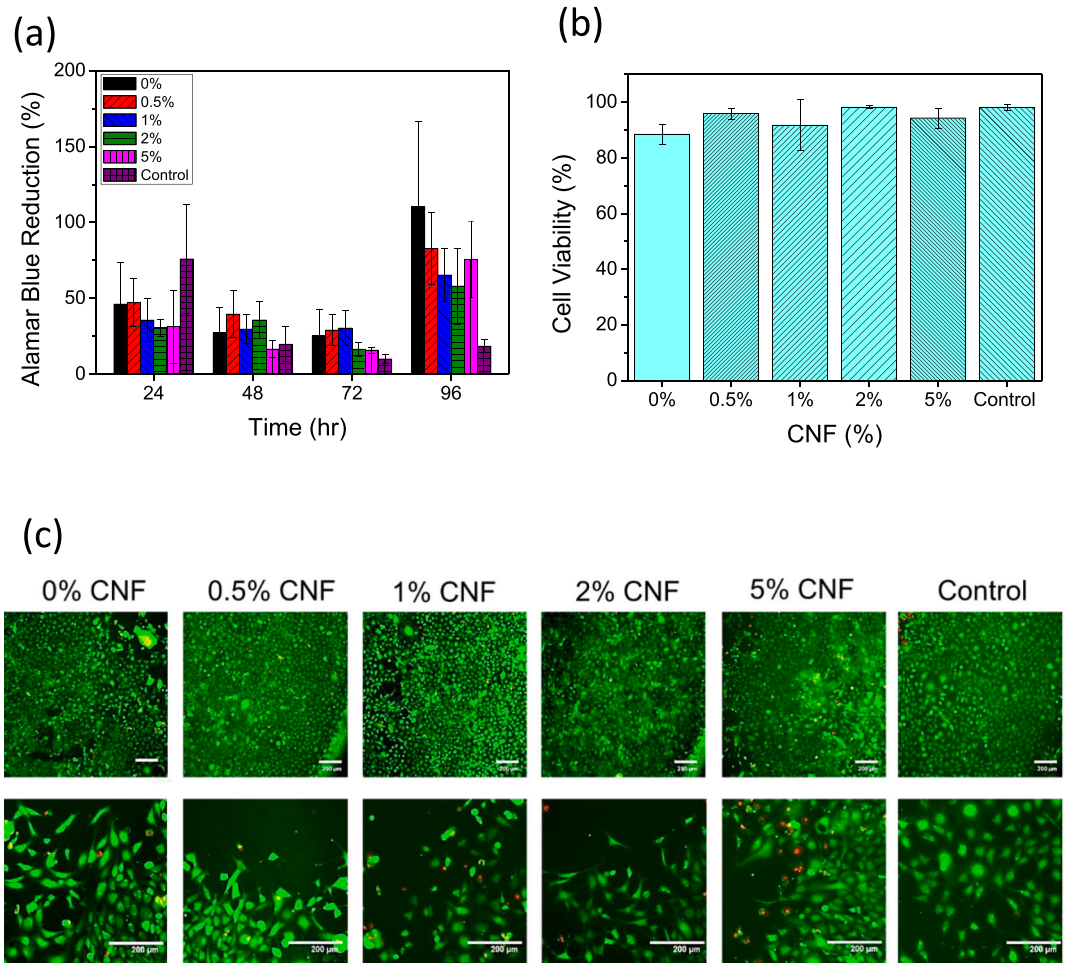

Fig. 8. (a) Alamar Blue reduction. (b) Percentage of live NIH/3T3 cells gathered from fluorescent images from (c). (c) LIVE-DEAD assay. For all tests NIH/3T3 cells were cultured in the presence of the alginate/gelatin/CNF hydrogels over a period of 96 h.

formation of a hydrogel with homogenously dispersed CNFs. Its rheological properties are well suited to printing and complex geometries can be obtained and retained via crosslinking. This allows mechanically robust structures to be printed, reaching Young's moduli of 534.75 ± 2.7 kPa. These hydrogels also exhibit electroactivity, with conductivity reaching $4.1 \times 10^{-4} \pm 2 \times 10^{-5}$ S/cm. Cell cytotoxicity studies with NIH /3T3 fibroblasts indicate that these hybrid systems are biocompatible and can enhance cellular attachment and proliferation. These hydrogels offer a future pathway for the development of electroactive inks for a variety of tissue types.

CRediT authorship contribution statement

Aleksandra Serafin: Data curation, funding acquisition, Writing - Original draft preparation, Software Caoimhe Murphy.: Data curation, Writing - Original draft preparation. Mario Culebras: Data curation, Writing - Original draft preparation, Investigation, Supervision. Maurice N Collins: Supervision, Validation, resources, project administration, Writing - Reviewing and editing,

Declaration of competing interest

The authors declare that they have no known competing financial interests or personal relationships that could have appeared to influence the work reported in this paper.

Acknowledgments

The authors would like to acknowledge the Irish Research Council (Project ID–EPSPG/2020/78). The authors also wish to acknowledge Miriama Ceresnakova from the Bernal Institute, Ireland for kindly agreeing to capture the cell viability of the NIH/3T3 cells with fluorescent confocal imaging.

References

[1] Keeping kidneys, Bulletin of the World Health Organization 90 (10) (2012) 718–719.
[2] S. Giwa, et al., The promise of organ and tissue preservation to transform medicine, Nat. Biotechnol. 35 (6) (2017) 530–542.
[3] F. Ullah, et al., Classification, processing and application of hydrogels: a review, Mater. Sci. Eng. C 57 (2015) 414–433.
[4] M.N. Collins, C. Birkinshaw, Hyaluronic acid based scaffolds for tissue engineering—a review, Carbohydr. Polym. 92 (2) (2013) 1262–1279.
[5] Y.-J. Seol, et al., Chitosan sponges as tissue engineering scaffolds for bone formation, Biotechnol. Lett. 26 (13) (2004) 1037–1041.
[6] A. Saarai, et al., On the development and characterisation of crosslinked sodium alginate/gelatine hydrogels, J. Mech. Behav. Biomed. Mater. 18 (2013) 152–166.
[7] F. Zamboni, et al., Enhanced cell viability in hyaluronic acid coated poly(lactic-co-glycolic acid) porous scaffolds within microfluidic channels, Int. J. Pharm. 532 (1) (2017) 595–602.
[8] J.A. Rowley, G. Madlambayan, D.J. Mooney, Alginate hydrogels as synthetic extracellular matrix materials, Biomaterials 20 (1) (1999) 45–53.
[9] M.D. Giuseppe, et al., Mechanical behaviour of alginate-gelatin hydrogels for 3D bioprinting, J. Mech. Behav. Biomed. Mater. 79 (2018) 150–157.
[10] T. Jiang, et al., Engineering bioprintable alginate/gelatin composite hydrogels with tunable mechanical and cell adhesive properties to modulate tumor spheroid growth kinetics, Biofabrication 10 (2019), 015024.
[11] H. Yu, et al., Effects of 3-dimensional bioprinting alginate/gelatin hydrogel scaffold extract on proliferation and differentiation of human dental pulp stem cells, J. Endod. 45 (6) (2019) 706–715.
[12] C.D. McCaig, M. Zhao, Physiological electrical fields modify cell behaviour 19 (9) (1997) 819–826.
[13] M. Hu, et al., Electrical stimulation enhances neuronal cell activity mediated by Schwann cell derived exosomes, Sci. Rep. 9 (1) (2019).
[14] T.A. Banks, et al., Effects of electric fields on human mesenchymal stem cell behaviour and morphology using a novel multichannel device, Integr. Biol. (Camb.) 7 (6) (2015) 693–712.
[15] A. Saberi, et al., Electrically conductive materials: opportunities and challenges in tissue engineering, Biomolecules 9 (9) (2019) 448.
[16] A. Vashist, et al., Advances in carbon nanotubes-hydrogel hybrids in nanomedicine for therapeutics, Adv. Healthcare Mater. 7 (2018) 9, 1701213.
[17] A. Alam, et al., Polymer composite hydrogels containing carbon nanomaterials—morphology and mechanical and functional performance, Prog. Polym. Sci. 77 (2018) 1–18.
[18] M. Llorens-Gámez, Á. Serrano-Aroca, Low-cost advanced hydrogels of calcium alginate/carbon nanofibers with enhanced water diffusion and compression properties, Polymers 10 (4) (2018) 405.
[19] P. Hu, et al., Network single-walled carbon nanotube biosensors for fast and highly sensitive detection of proteins 22 (33) (2011) 335502.
[20] P.D. Boyer, et al., Enhanced intracellular delivery of small molecules and drugs via non-covalent ternary dispersions of single-wall carbon nanotubes 4 (7) (2016) 1324–1330.
[21] B. Gorain, et al., Carbon nanotube scaffolds as emerging nanoplatform for myocardial tissue regeneration: a review of recent developments and therapeutic implications, Biomed. Pharmacother. 104 (2018) 496–508.
[22] S. Ahadian, et al., Hybrid hydrogels containing vertically aligned carbon nanotubes with anisotropic electrical conductivity for muscle myofiber fabrication, Sci. Rep. 4 (1) (2015).
[23] S.-J. Lee, et al., 3D printing nano conductive multi-walled carbon nanotube scaffolds for nerve regeneration, J. Neural Eng. 15 (1) (2018) 016018.
[24] M.H.R. Zadeh, et al., A comprehensive in vitro study of the carbon nanotube enhanced chitosan scaffolds for cancellous bone regeneration, Biomed. Phys. Eng. Express 4 (3) (2018), 035027.
[25] H.F. Cui, et al., Interfacing carbon nanotubes with living mammalian cells and cytotoxicity issues, Chem. Res. Toxicol. 23 (7) (2010) 1131–1147.
[26] C. Ruiz-Cornejo Juan, D. Sebastián, J. Lázaro Maria, Synthesis and applications of carbon nanofibers: a review, Rev. Chem. Eng. 36 (2018) 4, https://doi.org/10.1515/revce-2018-0021.
[27] M. Culebras, et al., Bio-derived carbon nanofibres from lignin as high-performance Li-ion anode materials, ChemSusChem 12 (19) (2019) 4516–4521.
[28] C.A. Murphy, et al., Biopolymers and polymers in the search of alternative treatments for meniscal regeneration: state of the art and future trends, Appl. Mater. Today 12 (2018) 51–71.
[29] H. Li, S. Liu, L. Lin, Rheological study on 3D printability of alginate hydrogel and effect of graphene oxide, Int. J. Bioprint. 2 (2) (2016).
[30] L. Feng, N. Xie, J. Zhong, Carbon nanofibers and their composites: a review of synthesizing, properties and applications, Materials (Basel, Switzerland) 7 (5) (2014) 3919–3945.
[31] X. Liu, et al., Electrically conductive nanocomposite hydrogels embedded with functionalized carbon nanotubes for spinal cord injury, New J. Chem. 42 (21) (2018) 17671–17681.
[32] X. Liu, et al., Functionalized carbon nanotube and graphene oxide embedded electrically conductive hydrogel synergistically stimulates nerve cell differentiation, ACS Appl. Mater. Interfaces 9 (17) (2017) 14677–14690.
[33] G. Lawrie, et al., Interactions between alginate and chitosan biopolymers characterized using FTIR and XPS, Biomacromolecules 8 (8) (2007) 2533–2541.
[34] A. Pielesz, M.K.K. Bąk, Raman spectroscopy and WAXS method as a tool for analysing ion-exchange properties of alginate hydrogels 43 (5) (2008) 438–443.
[35] W. Smolka, et al., Structure and biological properties of surface-engineered carbon nanofibers, J. Nanomater. 2019 (2019).
[36] Y.M. Ahmed, et al., Synthesis and characterization of carbon nanofibers grown on powdered activated carbon, J. Nanotechnol. 2016 (2016).
[37] K.Y. Lee, D.J. Mooney, Alginate: properties and biomedical applications, Prog. Polym. Sci. 37 (1) (2012) 106–126.
[38] M.S. Shoichet, et al., Stability of hydrogels used in cell encapsulation: an in vitro comparison of alginate and agarose, Biotechnol. Bioeng. 50 (4) (1996) 374–381.
[39] R. Urruela-Barrios, et al., Alginate/gelatin hydrogels reinforced with TiO_2 and β-TCP fabricated by microextrusion-based printing for tissue regeneration, Polymers 11 (3) (2019) 457.
[40] V. Kuzmenko, et al., Enhanced growth of neural networks on conductive cellulose-derived nanofibrous scaffolds, Mater. Sci. Eng. C 58 (2016) 14–23.
[41] W. Zhu, et al., Enhanced neural stem cell functions in conductive annealed carbon nanofibrous scaffolds with electrical stimulation, Nanomedicine 14 (7) (2018) 2485–2494.
[42] E.M. Steel, J.-Y. Azar, H.G. Sundararaghavan, Electrospun hyaluronic acid-carbon nanotube nanofibers for neural engineering, Materialia 9 (2020) 100581.